

Spin transport through a magnetic quantum wire: Dominance of spin inversion

Moumita Dey¹, Santanu K. Maiti^{1,2} and S. N. Karmakar¹

¹Theoretical Condensed Matter Physics Division,

Saha Institute of Nuclear Physics, 1/AF, Bidhannagar, Kolkata-700 064, India

²Department of Physics, Narasinha Dutt College, 129 Belilious Road, Howrah-711 101, India

We propose that a magnetic quantum wire composed of magnetic atomic sites can be used as a spin flipper depending on the system size. We adopt a simple tight-binding Hamiltonian to describe the model where the quantum wire is attached to two semi-infinite one-dimensional non-magnetic electrodes. Based on single particle Green's function formalism all the calculations are performed numerically which describe two-terminal conductance and current through the wire. Our exact results may be helpful in fabricating mesoscopic or nano-scale spin devices.

PACS numbers: 73.63.-b, 73.63.Rt, 73.63.Nm

I. INTRODUCTION

Over the past two decades spin dependent transport in low-dimensional systems has emerged as one of the most extensively cultivated area in condensed matter physics, due to its potential application in the fields of nanoelectronics and nanotechnology [1, 2]. Introduced in 1996, by S. Wolf, the term 'spintronics' [3–5] refers to a new branch in physics that deals with control and manipulation of electron spin in addition to its charge for storage and transfer of information as in conventional electronics. Idea of possibility to exploit electron spin in transport phenomena was ignited by the discovery of giant magneto-resistance (GMR) effect [6] in Fe/Cr magnetic multi-layers in 1980's and it holds future promises of integrating memory and logic into a single device. Since the discovery of GMR based magnetic field sensors, revolutionary development has taken place in magnetic data storage applications, device processing techniques, and quantum computation. 'Spintronics' presents a new paradigm in quantum computation with incredible speed up in computational time and much reduced complexity in quantum-computing algorithm, using the idea of quantum coherence and spin entanglement. The key idea of spintronic applications involves three basic steps that are injection of spin through interfaces, transmission of spin through matter, and finally detection of spin. Having considerably larger spin diffusion length molecules and quantum confined nanostructures e.g., quantum dots are ideal candidates to study spin dependent transmission. Therefore, from technological as well as theoretical point of view study of spin transport in mesoscopic regime is of great importance today.

Till date several experimental and theoretical works have been done to investigate spin transport phenomena at nanoscale level. In 2004 Rohkinson *et al.* prepared a spin filter [7] using GaAs by atomic force microscopy (AFM) with local anodic oxidation and molecular beam epitaxy methods. In 2005, gate field controlled magnetoresistance [8] in carbon nanotube with metallic contacts is observed by Schönenberger *et al.*. In 2007, Tombros *et al.* studied spin transport in single graphene

layer at room temperature [9]. Various other experiments have also been performed in this field. Along with such novel experimental works spin transport in mesoscopic regime has drawn attention from theoretical point of view also. Present theoretical investigations in this field explores various interesting features e.g., spin dependent conductance modulation [10], spin filtering [11], spin switching [12], spin detecting mechanisms [13], etc. Recently, Shokri *et al.* have studied spin dependent transmission within the coherent transport regime through magnetic or non-magnetic nanostructures e.g., quantum wire, etc. attached to semi-infinite magnetic or non-magnetic leads using Transfer matrix method and single particle Green's function formalism [14–18]. It is observed that the conductance of such mesoscopic systems depends on the spin state of electrons passing through the system and can be controlled by applying external magnetic field [19].

The aim of our present work is to study spin dependent transmission through a magnetic quantum wire. This system, composed of an array of magnetic atoms, is attached symmetrically to two non-magnetic (NM) semi-infinite one-dimensional (1D) metallic electrodes. A simple tight-binding Hamiltonian is used to describe the system where all the calculations are done by using single particle Green's function formalism. With the help of Landauer conductance formula [20, 21] spin dependent conductance is obtained, and the current-voltage characteristics are computed from the Landauer-Büttiker formalism [22–24]. We explore various features of spin dependent transport using different configurations of this simple geometry. It is interesting to note that for a specific configuration as we will describe later, spin flip transmission dominates significantly over pure spin transmission after the system size becomes larger than a critical value.

The scheme of the paper is as follow. With a brief introduction (Section I), in Section II, we describe the model and theoretical formulations for the calculation. Section III explores the significant results which describe two-terminal conductance and current through the wire and our results clearly depict the spin flipping action depending on the system size. At the end, we conclude our

study in Section IV.

II. MODEL AND SYNOPSIS OF THE THEORETICAL FORMULATION

We start by describing our model as shown in Fig 1. In this figure we illustrate schematically the 1D nanostructure through which we are interested to explore several features of spin dependent transport phenomena. In the present work, spin transmission is investigated through a

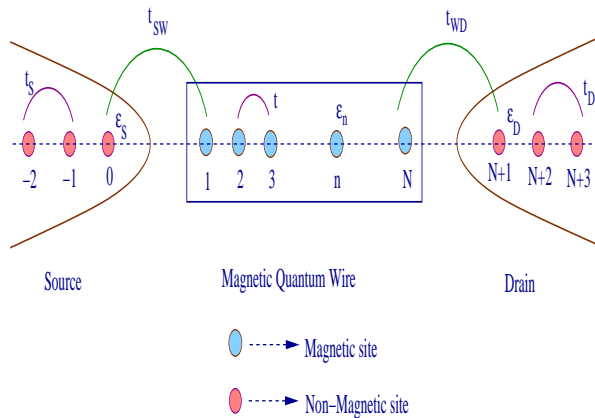
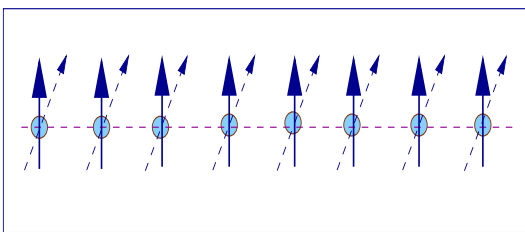


FIG. 1: (Color online). A magnetic quantum wire (framed region) of N atomic sites attached to two semi-infinite one-dimensional non-magnetic metallic electrodes, namely, source and drain. The filled sky blue circles correspond to the magnetic atomic sites in the quantum wire, while the filled pink circles represent the non-magnetic atomic sites comprising the electrodes.

magnetic quantum wire (MQW) which is basically an array of N number of magnetic atomic sites. Each site has a localized magnetic moment of equal amplitude associated with it. The orientations of the local magnetic moment in a site n (say) are specified by the polar angle θ_n and azimuthal angle ϕ_n in spherical polar coordinate system



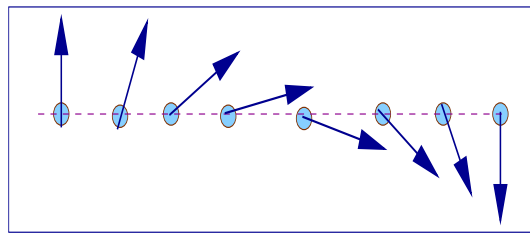
Configuration 1

FIG. 2: (Color online). Configuration 1: A magnetic quantum wire with N atomic sites where all magnetic moments are aligned in a particular direction (solid arrows). These moments are rotated equally from their initial directions by applying an external magnetic field (dashed arrows).

and the direction of the moment can be altered by apply-

ing an external magnetic field. The QW is attached symmetrically to two 1D semi-infinite non-magnetic metallic electrodes, commonly termed as source and drain having chemical potentials μ_1 and μ_2 under the non-equilibrium condition when bias voltage is applied. Described by the discrete lattice model, the electrodes are assumed to be composed of infinite non-magnetic sites labeled as $0, -1, -2, \dots, -\infty$ for the left electrode and $(N+1), (N+2), (N+3), \dots, \infty$ for the right one.

In our present work we consider two different configurations of the MQW depending on the orientation of the localized moments on each site as illustrated in Figs. 2 and 3. In configuration 1, (see Fig 2) all the magnetic moments are directed along $+Z$ direction and their ori-



Configuration 2

FIG. 3: (Color online). Configuration 2: A magnetic quantum wire with N atomic sites where the magnetic moments are oriented in a wave like pattern. The moments in sites 1 and N are oppositely oriented.

entation can be changed in an equal amount by applying an external magnetic field. In configuration 2 (see Fig 3) the magnetic moments are aligned in a spin wave like pattern with the help of a spatially inhomogeneous external magnetic field.

The Hamiltonian for the whole system can be written as,

$$H = H_W + H_S + H_D + H_{SW} + H_{WD} \quad (1)$$

where, H_W represents the Hamiltonian for the magnetic quantum wire (MQW). $H_{S(D)}$ corresponds to the Hamiltonian for the left (right) electrode, namely, source (drain), and $H_{SW(WD)}$ is the Hamiltonian describing the wire-electrode coupling.

The spin polarized Hamiltonian for the MQW can be written in a single electron picture within the framework of tight-binding formulation in Wannier basis, using nearest-neighbor approximation as,

$$H_W = \sum_{n=1}^N \mathbf{c}_n^\dagger \left(\epsilon_0 - \mathbf{h}_n \cdot \vec{\sigma} \right) \mathbf{c}_n + \sum_{i=1}^N \left(\mathbf{c}_i^\dagger \mathbf{t} \mathbf{c}_{i+1} + \text{h.c.} \right) \quad (2)$$

where,

$$\mathbf{c}_n^\dagger = \left(c_{n\uparrow}^\dagger \ c_{n\downarrow}^\dagger \right)$$

$$\begin{aligned} \mathbf{c}_n &= \begin{pmatrix} c_{n\uparrow} \\ c_{n\downarrow} \end{pmatrix} \\ \epsilon_0 &= \begin{pmatrix} \epsilon_0 & 0 \\ 0 & \epsilon_0 \end{pmatrix} \\ \mathbf{t} &= t \begin{pmatrix} 1 & 0 \\ 0 & 1 \end{pmatrix} \\ \vec{\mathbf{h}}_n \cdot \vec{\sigma} &= h_n \begin{pmatrix} \cos \theta_n & \sin \theta_n e^{-i\phi_n} \\ \sin \theta_n e^{i\phi_n} & -\cos \theta_n \end{pmatrix} \end{aligned}$$

First term of Eq. (2) represents the effective on-site energies of the atomic sites in the wire. ϵ_0 's are the site energies, while the term $\vec{\mathbf{h}}_n \cdot \vec{\sigma}$ describes the interaction of the spin (σ) of the injected electron with the localized on site magnetic moments. On-site flipping of spins is described mathematically by this term. Second term describes the nearest-neighbor hopping strength between the sites of the quantum wire.

Similarly, the Hamiltonian $H_{S(D)}$ for the two electrodes can be written as,

$$H_{S(D)} = \sum_i \mathbf{c}_i^\dagger \epsilon_{S(D)} \mathbf{c}_i + \sum_i \left(\mathbf{c}_i^\dagger \mathbf{t}_{S(D)} \mathbf{c}_{i+1} + \text{h.c.} \right) \quad (3)$$

where, $\epsilon_{S(D)}$'s are the site energies of source (drain) and $t_{S(D)}$ is the hopping strength between the nearest-neighbor sites of source (drain).

Here also,

$$\begin{aligned} \epsilon_{S(D)} &= \begin{pmatrix} \epsilon_{S(D)} & 0 \\ 0 & \epsilon_{S(D)} \end{pmatrix} \\ \mathbf{t}_{S(D)} &= \begin{pmatrix} t_{S(D)} & 0 \\ 0 & t_{S(D)} \end{pmatrix} \end{aligned}$$

The wire-electrode coupling Hamiltonian is described by,

$$H_{SW(WD)} = \left(\mathbf{c}_{0(N)}^\dagger \mathbf{t}_{SW(WD)} \mathbf{c}_{1(N+1)} + \text{h.c.} \right) \quad (4)$$

where, $t_{SW(WD)}$ being the wire-electrode coupling strength.

In order to calculate the spin dependent transmission probabilities and the current through the magnetic quantum wire we use single particle Green's function technique. Within the regime of coherent transport and for non-interacting systems this formalism is well applied.

The single particle Green's function representing the full system for an electron with energy E is defined as [20, 21],

$$\mathbf{G} = (\mathbf{E} - \mathbf{H})^{-1} \quad (5)$$

where,

$$\mathbf{E} = (\epsilon + i\eta)\mathbf{I} \quad (6)$$

In the above expression $i\eta$ is a small imaginary term added to the energy ϵ to make the Green's function \mathbf{G} non-hermitian.

Now, \mathbf{H} and \mathbf{G} representing the Hamiltonian and the Green's function for the full system those can be partitioned in terms of different sub-Hamiltonians like [20, 21],

$$\mathbf{H} = \begin{pmatrix} \mathbf{H}_S & \mathbf{H}_{SW} & 0 \\ \mathbf{H}_{SW}^\dagger & \mathbf{H}_W & \mathbf{H}_{WD} \\ 0 & \mathbf{H}_{WD}^\dagger & \mathbf{H}_D \end{pmatrix} \quad (7)$$

$$\mathbf{G} = \begin{pmatrix} \mathbf{G}_S & \mathbf{G}_{SW} & 0 \\ \mathbf{G}_{SW}^\dagger & \mathbf{G}_W & \mathbf{G}_{WD} \\ 0 & \mathbf{G}_{WD}^\dagger & \mathbf{G}_D \end{pmatrix} \quad (8)$$

where, \mathbf{H}_S , \mathbf{H}_D and \mathbf{H}_W represent the Hamiltonians (in matrix form) for source, quantum wire and drain, respectively. \mathbf{H}_{SW} and \mathbf{H}_{WD} are the matrices for the Hamiltonians representing the wire-electrode coupling. Assuming that there is no direct coupling between the electrodes themselves, the corner elements of the matrices are zero. A similar definition goes for the Green's function matrix \mathbf{G} as well.

Our first goal is to determine \mathbf{G}_W (Green's function for the wire only) which defines all physical quantities of interest. Following Eq. (5) and using the block matrix form of \mathbf{H} and \mathbf{G} the form of \mathbf{G}_W can be expressed as,

$$\mathbf{G}_W = (\mathbf{E} - \mathbf{H}_W - \Sigma_S - \Sigma_D)^{-1} \quad (9)$$

where, Σ_S and Σ_D represent the contact self-energies introduced to incorporate the effects of semi-infinite electrodes coupled to the system, and, they are expressed by the relations [20, 21],

$$\begin{aligned} \Sigma_S &= \mathbf{H}_{SW}^\dagger \mathbf{G}_S \mathbf{H}_{SW} \\ \Sigma_D &= \mathbf{H}_{WD}^\dagger \mathbf{G}_D \mathbf{H}_{WD} \end{aligned} \quad (10)$$

Thus, the form of self-energies are independent of the nano-structure itself through which transmission is studied and they completely describe the influence of electrodes attached to the system. Now, the transmission probability ($T_{\sigma\sigma'}$) of an electron with energy E is related to the Green's function as,

$$\begin{aligned} T_{\sigma\sigma'} &= \Gamma_{S(\sigma\sigma)}^1 \mathbf{G}_r^{1N} \mathbf{G}_a^{N1} \Gamma_{D(\sigma'\sigma')}^N \\ &= \Gamma_{S(\sigma\sigma)}^1 |\mathbf{G}_{(\sigma\sigma')}^{1N}|^2 \Gamma_{D(\sigma'\sigma')}^N \end{aligned} \quad (11)$$

where, $\Gamma_{S(\sigma\sigma)}^1 = \langle 1\sigma | \Gamma_S | 1\sigma \rangle$, $\Gamma_{D(\sigma'\sigma')}^N = \langle N\sigma' | \Gamma_D | N\sigma' \rangle$ and $\mathbf{G}_{\sigma\sigma'}^{1N} = \langle 1\sigma | \mathbf{G} | N\sigma' \rangle$. Here, \mathbf{G}_r and \mathbf{G}_a are the retarded and advanced single particle Green's functions (for the MQW only) for an electron with energy E . Γ_S and Γ_D are the coupling matrices, representing the coupling of the magnetic quantum wire to source and drain, respectively, and they are defined by the relation [20, 21],

$$\Gamma_{S(D)} = i[\Sigma_{S(D)}^r - \Sigma_{S(D)}^a] \quad (12)$$

Here, $\Sigma_{S(D)}^r$ and $\Sigma_{S(D)}^a$ are the retarded and advanced self-energies, respectively, and they are conjugate to each

other. It is shown in literature by Datta *et al.* that the self-energy can be expressed as a linear combination of a real and an imaginary part in the form,

$$\Sigma_{\mathbf{S}(\mathbf{D})}^r = \Lambda_{\mathbf{S}(\mathbf{D})} - i\Delta_{\mathbf{S}(\mathbf{D})} \quad (13)$$

The real part of self-energy describes the shift of the energy levels and the imaginary part corresponds to broadening of the levels. The finite imaginary part appears due to incorporation of the semi-infinite electrodes having continuous energy spectrum. Therefore, the coupling matrices can easily be obtained from the self-energy expression and is expressed as,

$$\Gamma_{\mathbf{S}(\mathbf{D})} = -2\text{Im}(\Sigma_{\mathbf{S}(\mathbf{D})}) \quad (14)$$

Considering linear transport regime, conductance (g_σ) is obtained using Landauer formula [20, 21],

$$g_{\sigma\sigma'} = \frac{e^2}{h} T_{\sigma\sigma'} \quad (15)$$

Knowing the transmission probability ($T_{\sigma\sigma'}$) of an electron injected with spin σ and transmitted with spin σ' , the current ($I_{\sigma\sigma'}$) through the system is obtained using Landauer-Büttiker formalism. It is written in the form [20, 21],

$$I_{\sigma\sigma'}(V) = \frac{e}{h} \int_{-\infty}^{+\infty} [f_L(E) - f_R(E)] T_{\sigma\sigma'}(E) dE \quad (16)$$

where, $f_{L(R)} = f(E - \mu_{L(R)})$ gives the Fermi distribution function of the two electrodes having chemical potentials $\mu_{L(R)} = E_F \pm eV/2$. E_F is the equilibrium Fermi energy.

III. NUMERICAL RESULTS AND DISCUSSION

We investigate various features of spin dependent transport through a magnetic quantum wire (MQW) for two different geometrical configurations depending on the orientations of the localized magnetic moments associated with each atom. In the first configuration, all the moments are aligned parallel to each other and initially they are chosen to be directed along $+Z$ direction, while in the second one the magnetic moments are oriented in a spin wave like pattern. All the results shown in the present work are obtained numerically. Therefore, we start analyzing the results by mentioning all the parameters that are used for numerical calculation. Our first assumption is that the two non-magnetic electrodes are made up of identical materials. The on-site energies in the wire ϵ_0 as well as in the leads ($\epsilon_{S(D)}$) are set as 0. Hopping strength between the sites in the two electrodes is chosen as $t_{S(D)} = 4$ whereas, in the QW it is set as $t = 4$. The equilibrium Fermi energy E_F is set at 0. Our unit system is simplified by choosing $\hbar = c = e = 1$.

Throughout the analysis we present the basic features of spin transport for two distinct regimes of electrode-to-MQW coupling. These regimes are described as follows.

Case 1: Weak-coupling limit

This limit is set by the criterion $t_{SW(WD)} \ll t$. In this case, we choose the values as $t_{SW} = t_{WD} = 0.5$.

Case 2: Strong-coupling limit

This limit is described by the condition $t_{SW(WD)} \sim t$. In this regime we choose the values of hopping strengths as $t_{SW} = t_{WD} = 2.5$.

A. Features of Spin Transport for Configuration 1

1. Conductance-Energy Characteristics

First, we plot the conductance-energy characteristics in the two coupling regimes specified above. In Fig. 4 we show the variation of conductance due to pure spin transmission ($g_{\uparrow\uparrow}$) and spin flip transmission ($g_{\uparrow\downarrow}$) with respect to the injecting electron energy E . In this figure, conductance due to pure spin transmission exhibits sharp reso-

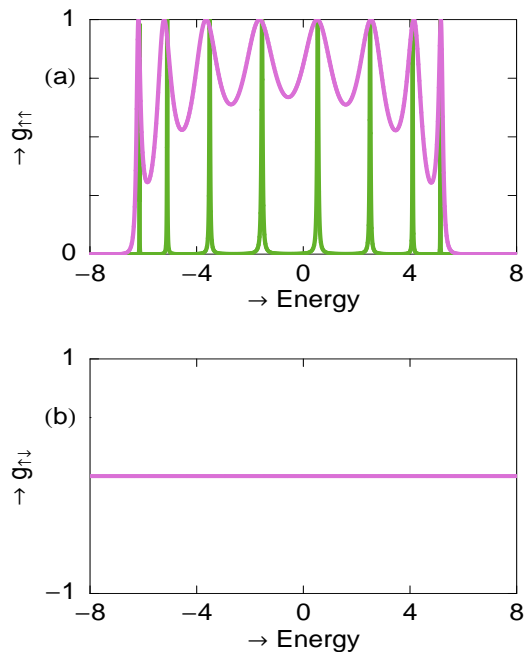


FIG. 4: (Color online). g - E characteristics for a magnetic quantum wire considering the system size $N = 8$ where all the moments are aligned along $+Z$ direction. The upper and lower panels describe the variations of $g_{\uparrow\uparrow}$ and $g_{\uparrow\downarrow}$, respectively. The green and pink curves represent the results for the weak- and strong-coupling limits, respectively.

nant peaks at some discrete energy values in the weak-coupling limit, whereas the peaks acquire some broadening in the limit of strong coupling. The conductance-energy characteristic reveals the feature of energy spectrum completely. The broadening of conductance peaks with the enhancement of coupling strength is quantified by the imaginary parts $\Delta_{\mathbf{S}}$ and $\Delta_{\mathbf{D}}$ of the self-energy

matrices Σ_S and Σ_D which are incorporated in the conductance expression via the coupling matrices [20, 21]. Conductance by spin flipping is zero for the entire energy region in this particular configuration as seen from Fig. 4(b), where the green and pink curves overlap to each other. The reason of zero spin flipping is explained in the forthcoming sub-section.

2. Variation of Conductance with Polar Angle θ

In Fig. 5 we plot the variation of conductance ($g_{\uparrow\uparrow}$ and $g_{\uparrow\downarrow}$) with the angle θ made by the magnetic moments with the preferred $+Z$ direction. It is evident from this figure that $g_{\uparrow\uparrow}$ exhibits 2π periodicity as a func-

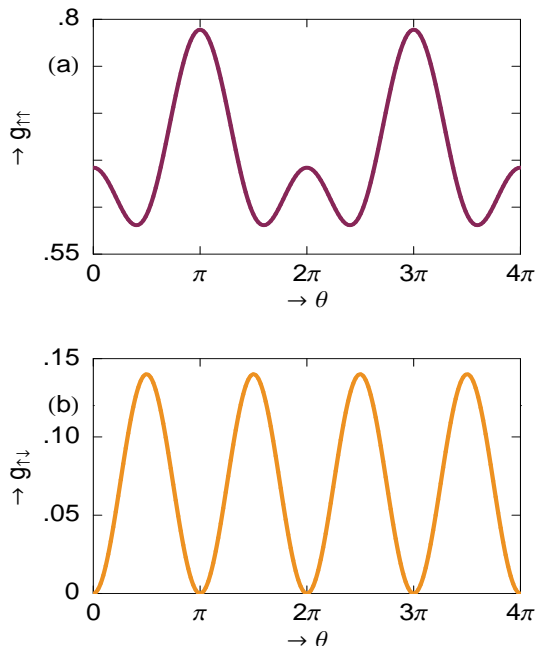


FIG. 5: (Color online). Variation of conductances with polar angle θ for a magnetic quantum wire considering $N = 8$. The upper and lower panels correspond to the cases of $g_{\uparrow\uparrow}$ and $g_{\uparrow\downarrow}$, respectively.

tion of θ , whereas, $g_{\uparrow\downarrow}$ shows π periodicity. Rotation of magnetic moments through an angle 2π map themselves into their initial positions. So 2π periodicity is expected in the variation of $g_{\uparrow\uparrow}$ with θ . On the other hand, the reason of π periodicity in the case of spin flip conductance ($g_{\uparrow\downarrow}$) can be explained in the following way. Occurrence of spin flipping is governed by the term $\vec{h}\cdot\vec{\sigma}$ in the Hamiltonian (see Eq. (2)), where, $\vec{\sigma}$ stands for the Pauli spin matrix having components σ_x , σ_y and σ_z for the injecting electron and h being the localized magnetic moments associated with each magnetic site in the quantum wire (QW). Spin flipping is mathematically expressed by the operation of raising ($\sigma_+ = \sigma_x + i\sigma_y$) and lowering ($\sigma_- = \sigma_x - i\sigma_y$) operators. For the local magnetic mo-

ments oriented along $\pm Z$ axis i.e., for $\theta = 0$ and π , $\vec{h}\cdot\vec{\sigma}$ ($= h_x\sigma_x + h_y\sigma_y + h_z\sigma_z$) becomes equal to $h_z\sigma_z$. Accordingly, the Hamiltonian does not contain σ_x and σ_y and so as σ_+ and σ_- , which provides zero flipping for up or down orientation of magnetic moments. Since, spin flip transmission drops exactly to zero when θ becomes an integer multiple of π , $g_{\uparrow\downarrow}$ provides π periodicity as a function of θ .

3. Current-Voltage Characteristics

All the essential features of spin transport described earlier to be more transparent from our current-voltage characteristics. Current through the MQW is computed by integrating over the transmission curve following Landauer-Büttiker formalism. Transmission probability varies in an exactly identical way to that of the

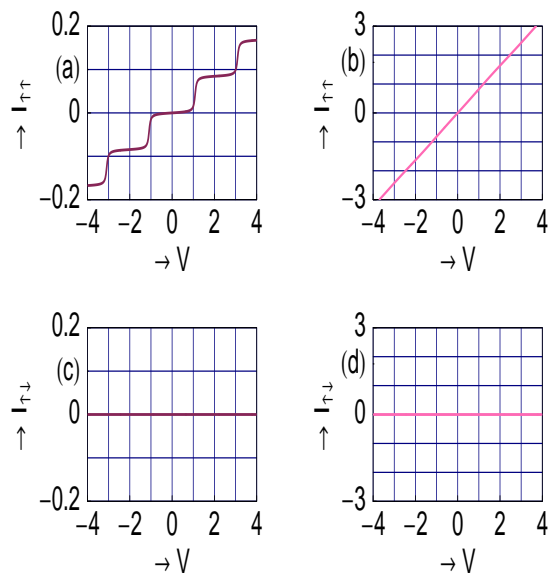


FIG. 6: (Color online). Current I as a function of applied bias voltage V for a magnetic quantum wire with $N = 8$ where all magnetic moments are aligned along $+Z$ direction. The left and right columns correspond to the cases of weak and strong wire to electrode coupling strengths, respectively.

conductance spectrum apart from a scale factor e^2/h (which is equal to 1 in our chosen unit system). The current $I_{\uparrow\uparrow}$ shows staircase like pattern due to the presence of sharp, discrete resonant peaks in the limit of weak-coupling. With the increase in applied bias voltage V , the difference in chemical potentials of the two electrodes ($\mu_1 - \mu_2$) increases, allowing more number of energy levels to fall in that range, and accordingly, more energy channels are accessible to the injected electrons to pass through the magnetic quantum wire from the source to drain. Incorporation of a single discrete energy level i.e., a discrete quantized conduction channel, between the

range ($\mu_1 - \mu_2$) provides a jump in the I - V characteristics. Contribution to the current $I_{\uparrow\downarrow}$ due to spin flipping is zero as the spin flip transmission probability is zero for this configuration.

In the limit of strong wire-electrode coupling, due to the broadening of conductance peaks current $I_{\uparrow\downarrow}$ shows nearly ohmic behavior as a function of applied bias voltage V . Enhancement in coupling strength does not change spin flip transmission probability.

B. Features of Spin Transport for Configuration 2

1. Conductance-Energy Characteristics

In Fig. 7 we plot the variation of conductance due to pure transmission ($g_{\uparrow\uparrow}$) and spin flip transmission ($g_{\uparrow\downarrow}$)

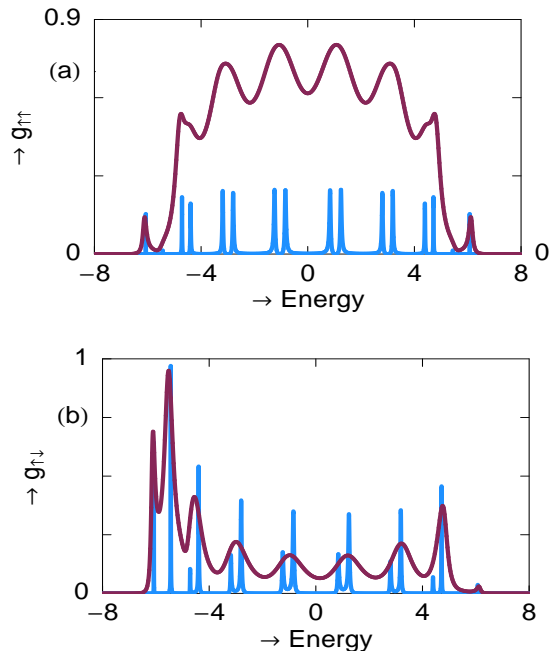


FIG. 7: (Color online). g - E characteristics for a magnetic quantum wire considering the system size $N = 8$ where the magnetic moments are aligned according to configuration 2 (Fig. 3). The upper and lower panels describe the variations of $g_{\uparrow\uparrow}$ and $g_{\uparrow\downarrow}$, respectively. The blue and violet curves represent the results for the weak- and strong-coupling limits, respectively.

in both the weak- and strong-coupling regimes. Variation of $g_{\uparrow\uparrow}$ exhibits sharp peaks at some discrete energy values in the weak-coupling limit, while in the limit of strong-coupling they achieve substantial broadening. The effect of such broadening is clearly understood from our previous discussion. But for this type of configuration i.e., where the orientation of each magnetic moment is increased gradually with respect to the $+Z$ axis along the length of the quantum wire, conductance am-

plitude due to pure spin transmission ($g_{\uparrow\uparrow}$) in the limit of strong-coupling is sufficiently high than that of the weak-coupling case. This feature is clearly noticed by comparing two curves in Fig. 7(a). For this typical configuration we also observe non-zero conductance due to spin flip as given in Fig. 7(b).

2. Current-Voltage Characteristics

In Fig. 8 we show the variations of spin dependent currents $I_{\uparrow\uparrow}$ and $I_{\uparrow\downarrow}$ as a function of applied bias voltage V for a magnetic quantum wire considering the system size $N = 8$. All the basic features of currents are same as we

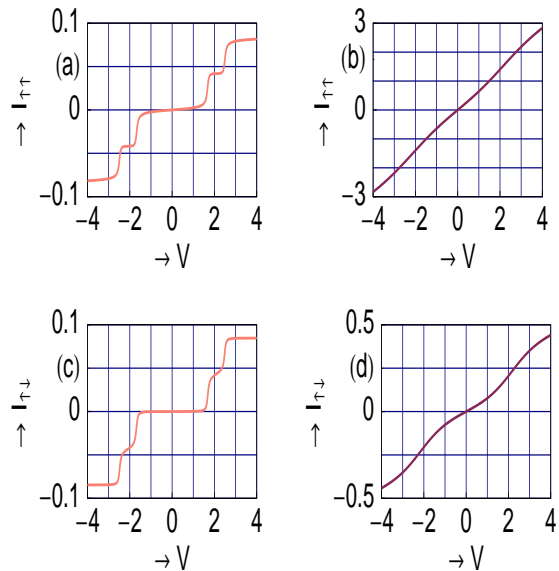


FIG. 8: (Color online). Current I as a function of applied bias voltage V for a magnetic quantum wire with $N = 8$ where the magnetic moments are aligned according to configuration 2 (Fig. 3). The left and right columns correspond to the cases of weak and strong wire to electrode coupling strengths, respectively.

observe in the case of configuration 1 e.g., step-like behavior in the weak-coupling limit and almost linear variation with larger amplitude in the limit of strong-coupling. But the notable signatures for this configuration are non-zero current due to spin flipping $I_{\uparrow\downarrow}$, and comparable amplitude of $I_{\uparrow\uparrow}$ and $I_{\uparrow\downarrow}$ in the weak-coupling limit for this system size.

3. Variation of Conductance with System Size N

Finally, in Fig. 9 we present the variations of $g_{\uparrow\uparrow}$ and $g_{\uparrow\downarrow}$ with system size N in the limit of strong-coupling. The conductances are calculated at the typical energy $E = 1.5$. For such configuration $g_{\uparrow\downarrow}$ increases gradually with system size N , while $g_{\uparrow\uparrow}$ decreases with the rise of

N . For this configuration, the magnetic moments are oriented sequentially from 0 to π and from earlier discussion it is evident that spin flip does occur when the magnetic moments are oriented at an angle θ with respect to the preferred $+Z$ direction. Hence, for the configuration 2, $g_{\uparrow\downarrow}$ increases with system size due to large number of se-

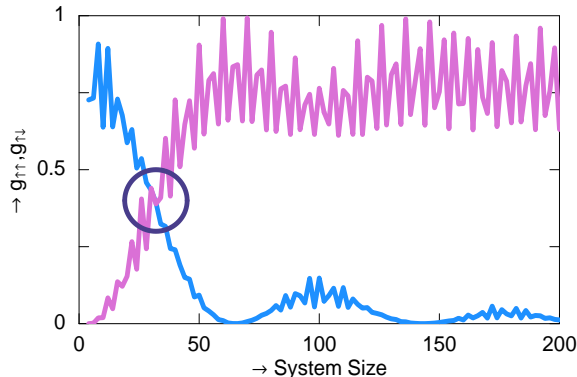


FIG. 9: (Color online). Variations of $g_{\uparrow\uparrow}$ and $g_{\uparrow\downarrow}$ with system size N for the typical energy $E = 1.5$ in the limit of strong wire-electrode coupling. The blue and pink curves correspond to the features of $g_{\uparrow\uparrow}$ and $g_{\uparrow\downarrow}$, respectively.

quential spin flip scattering and after a critical system size marked by the violet circle in Fig. 9, spin flip transmission dominates significantly over pure spin transmission. A similar feature is also observed in the case of weak-coupling limit, and therefore, here we do not show the results for this coupling limit further.

IV. CLOSING REMARKS

In a nutshell, in the present work we study spin dependent transport through a magnetic quantum wire (MQW) using single particle Green's function technique. We have adopted a discrete lattice model in tight-binding framework to illustrate the system which is simply an array of identical magnetic atomic sites. In our theoretical study two different geometrical configurations of the MQW depending on the orientation of the magnetic moments associated with each magnetic site. In the first configuration, all the moments are aligned at an equal angle with respect to the $+Z$ axis, while in the second one the moments are sequentially oriented from angle 0

to π relative to the $+Z$ direction. Orientation of the magnetic moments can be changed by applying an external magnetic field.

First, we investigate the features of spin dependent transport through a MQW having configuration 1. We started with the study of spin dependent conductance ($g_{\uparrow\uparrow}$ and $g_{\uparrow\downarrow}$) as a function of injecting electron energy E in the limit of both weak and strong wire-electrode coupling strengths. Next, we have shown the dependence of $g_{\uparrow\uparrow}$ and $g_{\uparrow\downarrow}$ on the orientation of the localized moments. It is evident from the g - θ variation that spin flipping is blocked for magnetic moments oriented along $\pm Z$ axis. Finally, we have determined the I - V characteristics. We have plotted both $I_{\uparrow\uparrow}$ and $I_{\uparrow\downarrow}$ as a function of applied bias voltage V . This figure shows that increasing the coupling strength, current amplitude gets enhanced quite significantly. Next, we have explored the important signatures of spin transport using the specific geometry of configuration 2. For this configuration first we have observed the conductance-energy and current-voltage characteristics as we have discussed in the case of configuration 1. All the essential features were same except that for this configuration magnitude of spin flip transmission probability is comparable to that of pure spin transmission probability. In the last figure, we have plot the variations of $g_{\uparrow\uparrow}$ and $g_{\uparrow\downarrow}$ with the system size N for typical electron energy $E = 1.5$ in the limit of strong wire-electrode coupling, which is the most interesting part of our theoretical study. It clearly demonstrates that after a certain system size spin flip transmission dominates significantly over the pure spin transmission. For a sufficiently large system, spin inversion takes place most prominently which can be utilized for fabricating spin based nano devices.

In the present work we have calculated all these results by ignoring the effects of temperature, spin-orbit interaction, electron-electron correlation, electron-phonon interaction, disorder, etc. Here, we set the temperature at 0K, but the basic features will not change significantly even in non-zero finite (low) temperature region as long as thermal energy ($k_B T$) is less than the average energy spacing of the energy levels of the magnetic quantum wire. In this model it is also assumed that the two side-attached non-magnetic electrodes have negligible resistance.

All these predicted results using such simple geometric configurations may be useful in designing a spin based nano devices.

[1] J. Chen, M. A. Reed, A. M. Rawlett, and J. M. Tour, *Science* **286**, 1550 (1999).
 [2] P. Ball, *Nature (London)* **404**, 918 (2000).
 [3] S. A. Wolf *et al.*, *Science* **294**, 1488 (2001).
 [4] G. Prinz, *Science* **282**, 1660 (1998).
 [5] G. Prinz, *Phys. Today* **48**, 58 (1995).
 [6] M. N. Baibich, J. M. Broto, A. Fert, F. N. Van Dau,

F. Petroff, P. Etienne, G. Creuzet, A. Friederich, and J. Chazelas, *Phys. Rev. Lett.* **61**, 2472 (1998).
 [7] Rokhinson *et al.*, *Phys. Rev. Lett.* **93**, 146601 (2004).
 [8] Schönenberger *et al.*, *Nature Phys.* **1**, 99 (2005).
 [9] Tombros *et al.*, *Nature*. **448**, 571 (2007).
 [10] I. A. Shelykh, N. T. Bagraev, N. G. Galkin, and L. E. Klyanchkin, *Phys. Rev. B* **71**, 113311 (2005).

- [11] H. W. Wu, J. Zhou, and Q. W. Shi, Appl. Phys. Lett. **85**, 1012 (2004).
- [12] D. Frustaglia, M. Hentschel, and K. Richter, Phys. Rev. Lett. **87**, 256602 (2001).
- [13] R. Ionićoiu and I. D'Amico, Phys. Rev. B **67**, 041307(R) (2003).
- [14] A. A. Shokri, M. Mardaani, and K. Esfarjani, Physica E **27**, 325 (2005).
- [15] A. A. Shokri, M. Mardaani, and K. Esfarjani, Physica E **27**, 325 (2005).
- [16] A. A. Shokri and M. Mardaani, Solid State Commun. **137**, 53 (2006).
- [17] M. Mardaani and A. A. Shokri, Chem. Phys. **324**, 541 (2006).
- [18] A. A. Shokri and A. Daemi, Eur. Phys. J. B **69**, 245 (2009).
- [19] A. A. Shokri and A. Saffarzadeh, J. Phys.: Condens. Matter **16**, 4455 (2004).
- [20] S. Datta, *Electronic transport in mesoscopic systems*, Cambridge University Press, Cambridge (1997).
- [21] S. Datta, *Quantum Transport: Atom to Transistor*, Cambridge University Press, Cambridge (2005).
- [22] R. Landauer, Phys. Lett. A **85**, 91 (1986).
- [23] R. Landauer, IBM J. Res. Dev. **32**, 306 (1988).
- [24] M. Büttiker, IBM J. Res. Dev. **32**, 317 (1988).